

A Study of the Cutting Temperature in Milling Stainless Steels with Chamfered Main Cutting Edge Sharp Worn Tools

Chung-Shin Chang¹

Abstract: The main purpose of this paper is to study the carbide tip's surface temperature and the cutting forces of milling stainless steel with chamfered main cutting sharp worn tools. The carbide tip's mounting in the tool holder are ground to a wear depth that is measured by a toolmaker microscope and a new cutting temperature model incorporating tool wear factor and using the variations of shear and friction plane areas occurring in tool worn situations are presented in this paper. The tool tip and cutting edges are treated as a series of elementary cutting tips. The forces and frictional heat generated on elementary cutting tools are calculated by using the measured cutting forces and the oblique cutting analysis. The carbide tip's temperature distribution is solved by finite element analysis (FEM) method.

Keywords: Milling, stainless steel, cutting temperatures, FEM.

1 Introduction

Many experimental techniques for measuring the metal cutting temperatures can also be found in the literature Leshock and Shin (1997). The drawbacks of the many simplified assumptions associated with the analytical solutions were overcome by the finite element analysis (FEM) of Tay, Stevenson, de Vahl Davis, and Oxley (1976). Singamneni (2005) demonstrated that the mixed finite and boundary element model enabling the estimation of cutting temperatures is simple, efficient, and at the same time quite easily implemented. Chang (2007) also presented a force model and an FEM model that agreed in predicting the cutting temperatures for turning stainless steel with a sharp chamfered main cutting edge tool. The aim of this paper is to clarify the cutting temperatures and the cutting forces of stainless steel when the sharp chamfered main cutting edge tool is worn down.

¹ Department of Mechanical Engineering, National Ilan University, I-Lan, Taiwan, 26014.

2 Theoretical Analysis

Chang (2005) the basic force model for a sharp worn corner tool with a chamfered main cutting edge ($R = 0$) shown in Fig. 1 was derived as follows:

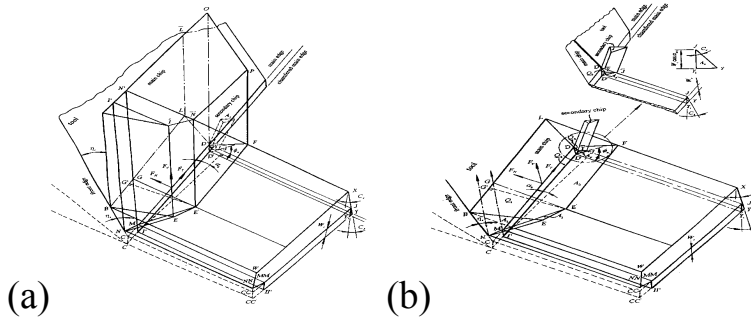


Figure 1: (a)Basic and (b)detailed model of the chamfered main cutting tool when wear occurs ($f > R, R = 0$)

Table 1: Tool geometry specifications (chamfered main cutting edge sharp worn tools)

side cutting edge angle	tool No.	positive and negative radial angles α_{r1}, α_{r2}	nose roundness (R)
20°	1	10°, -10° (10°, -10°)	0.0 (sharp and worn)
20°	2	20°, -20° (20°, -20°)	0.0 (sharp and worn)
20°	3	30°, -30° (30°, -30°)	0.0 (sharp and worn)
30°	4	10°, -10° (10°, -10°)	0.0 (sharp and worn)
30°	5	20°, -20° (20°, -20°)	0.0 (sharp and worn)
30°	6	30°, -30° (30°, -30°)	0.0 (sharp and worn)
40°	7	10°, -10° (10°, -10°)	0.0 (sharp and worn)
40°	8	20°, -20° (20°, -20°)	0.0 (sharp and worn)
40°	9	30°, -30° (30°, -30°)	0.0 (sharp and worn)
notation: tool holder and tips			

For the case of chamfered main cutting edge, temperatures and forces depend on nose radius R , worn depth d_B , cutting depth d , feed rate f , cutting speed V , positive radial angle α_{r1} , negative radial angle α_{r2} and axial angle α_d as shown in Table 1.

Fig. 1, C_s is the side cutting edge angle, C_e is the end cutting edge angle, α_{r1} and α_{r2} is used. The process for deriving the shear plane areas is divided into segments with tool wear and without wear.

Figures 2 reveals that the geometrical specification of tool wear on the tool face (triangle CNM) can be derived from the values of t_W and ϕ_A when already measured.

$$A = A_1 + A_2 + A_3 + A_s \quad (\text{as shown in Fig. 1a}) \quad (1)$$

$$A_1 = \frac{1}{2} a_3 b_3 \sin \theta_3 = \frac{1}{2} a_3 b_3 \left[1 - \frac{a_3^2 + b_3^2 - c_3^2}{2a_3 b_3} \right]^{1/2} \quad (A_1 = \Delta NBE) \quad (2)$$

$$A_2 = \frac{1}{2} (a_4 + b_4) \cdot h_4 \quad (A_2 = \text{retangle } MD FE') \quad (3)$$

$$A_3 = A_{31} + A_{32} \quad (A_3 = \Delta ME' E + \Delta MNE) \quad (4)$$

$$A_{31} = \frac{a_5 b_5}{2 \cos \phi_e} \sin \left(\frac{\frac{\pi}{2} + \alpha_b + \angle A31}{2} \right) \quad (5)$$

$$\angle A31 = \cos^{-1} \left[\frac{c_5^2 + d_5^2 - e_5^2}{2c_5 d_5} \right] \quad (6)$$

$$A_{32} = g_5 h_5 \frac{\sin(\angle A32)}{2 \cos \phi_e} \quad (7)$$

$$\angle A32 = \cos^{-1} \left[\frac{h_5^2 + n_5^2 - m_5^2}{2h_5 n_5} \right] - \sin^{-1} \left[\frac{l_5}{s_5} \sin \left(\frac{\pi}{2} - \alpha_a \right) \right] \quad (8)$$

$$A_s = \frac{1}{2} \frac{W_e^2 \cos^2 \alpha_{r1} \cdot \tan C_s}{\cos \alpha_a \sin \phi_e} \quad (A_s \text{ is the area of scendary chip: } \Delta D' \bar{Y} J) \quad (9)$$

$$Q = Q_1 + Q_2 + Q_3 \quad (10)$$

$$Q_1 = \frac{0.5(d/\cos C_s - W_e \cos \alpha_{r1} \tan C_s)}{\cos \alpha_a} \times \frac{f \cos C_s - W_e \cos \alpha_{r1}}{\cos \alpha_{r2}} - \frac{\overline{CN} \cdot \overline{NM} \sin \theta_B}{2} \quad (11)$$

$$Q_2 = \frac{W_e \cos \alpha_{r1} (d/\cos C_s - W_e \cos \alpha_{r1} \tan C_s)}{\cos \alpha_a} - (\overline{CN} \cdot W_e \cos \alpha_{r1}) \quad (12)$$

$$Q_3 = \frac{1}{2} \frac{W_e^2 \cos \alpha_{r1} \tan C_s}{\cos \alpha_a} \quad (Q_3 \text{ is the area of trangle } DD' \bar{Y}) \quad (13)$$

$$\overline{CM} = t_w (\cos C_s + \sin C_s \cdot \tan \theta_A) \tag{14}$$

$$\overline{CN} = \frac{t_w (\cos C_s + \sin C_s \cdot \tan \theta_A)}{(\sin \theta_A \tan \theta_A + \cos \theta_B)} \tag{15}$$

$$\overline{NM} = (\overline{CM}^2 + \overline{CN}^2 - 2\overline{CM} \cdot \overline{CN} \cos \theta_B)^{1/2} \tag{16}$$

$$\angle CMN = \cos^{-1} \left[\frac{(\overline{CM}^2 + \overline{CN}^2 - \overline{NM}^2)}{2\overline{CM} \cdot \overline{CN}} \right] \tag{17}$$

$$\angle CNM = \cos^{-1} \left[\frac{(\overline{CN}^2 + \overline{NM}^2 - \overline{CM}^2)}{2\overline{CN} \cdot \overline{NM}} \right] \tag{18}$$

Measurements are according to the setting location of the tool and the wear condition of the tool. The contact length of the tool edge can be considered as two types, as shown in Figs. 2 to 3.

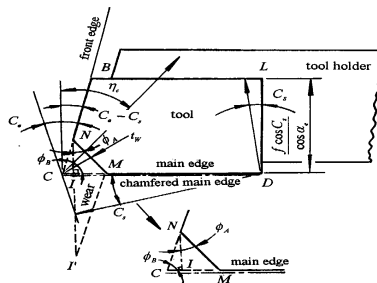


Figure 2: Specifications of tool with wear

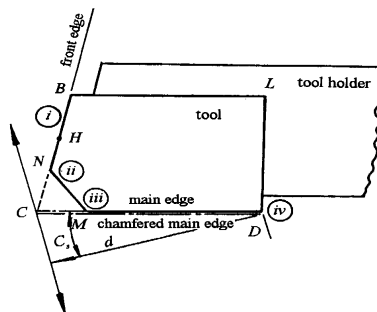


Figure 3: Contact length L_f and L_p with chamfered main cutting edge tool

From the above diagram, the contact length is

$$l_f = \overline{HN} + \overline{NM} + \overline{MD} = \bar{i} \cdot \bar{ii} + \bar{ii} \cdot \bar{iii} + \bar{iii} \cdot \bar{iv}$$

$$= \left[\frac{f \cos C_s / \cos \alpha_e - W_e \cos \alpha_{r1}}{\cos(C_e - C_s)} \right] + \overline{NM} + d / (\cos C_s \cos \alpha_a) - \overline{CM} \quad (19)$$

$$l_p = \overline{HN} \cos C_e + \overline{NM} \cos(\angle CNM - C_e) + \overline{MD} \sin C_s$$

$$= \frac{(f \cos C_s - W_e \cos \alpha_{r1}) \cos C_e}{\cos \alpha_e \cos(C_e - C_s)} + \overline{NM} \cos(\angle CNM - C_e) + \left(\frac{d}{\cos C_s} - \overline{CM} \right) \sin C_s \quad (20)$$

This situation is the same as Fig. 1, in which the shear area can be calculated. That is,

$$A = A_5 + A_6 + A_s \quad (21)$$

$$A_5 = \frac{1}{2} a_6 b_6 \left(1 - \frac{a_6^2 + b_6^2 - c_6^2}{2a_6 b_6} \right)^{1/2} \quad (22)$$

$$A_6 = \frac{1}{2} (e_6 + g_6) \cdot h_6 \quad (23)$$

$$A_s = \frac{1}{2} \frac{W_e^2 \cos^2 \alpha_{r1} \cdot \tan C_s}{\cos \alpha_a \sin \phi_e} \quad (A_s \text{ is the area of secondary chip: } \Delta D'YJ) \quad (24)$$

$$Q = Q_4 + Q_2 + Q_3 \quad (25)$$

$$Q_4 = 0.5 \left\{ \left[\frac{f \cos C_s}{\cos \alpha_e} - W_e \cos \alpha_{r1} \right] \tan \theta_A \right. \\ \left. + 2 \left[\frac{d}{\cos C_s} - \overline{CM} \right] \right\} \left(\frac{f \cos C_s}{\cos \alpha_e} - W_e \cos \alpha_{r1} \right) \quad (26)$$

$$Q_2 = \frac{W_e \cos \alpha_{r1} (d / \cos C_s - W_e \cos \alpha_{r1} \tan C_s)}{\cos \alpha_a} - (\overline{CN} \cdot W_e \cos \alpha_{r1}) \quad (27)$$

$$Q_3 = \frac{1}{2} \frac{W_e^2 \cos \alpha_{r1} \tan C_s}{\cos \alpha_a} \quad (28)$$

2.1 Energy method of predict cutting force

The shear energy per unit time U_s and the friction energy per unit U_f can be determined by the following equations.

$$U_s = F_s V_s = \frac{\tau_s A \cos \alpha_e}{\cos(\phi_e - \alpha_e)} V \quad (29)$$

$$U_f = F_t \cdot V_c = f_t \int_0^{B_1} db \cdot V_c = \frac{\tau_s \cdot \sin \beta \cdot \cos \alpha_e \cdot Q \cdot V}{[\cos(\phi_e + \beta - \alpha_e) \cdot \cos(\phi_e - \alpha_e)]} \quad (30)$$

$$F_s = \tau_s \cdot A; V_s = \frac{V \cos \alpha_e}{\cos(\phi_e - \alpha_e)}, V_c = \frac{V \sin \phi_e}{\cos(\phi_e - \alpha_e)} \quad (31)$$

$$U = U_s + U_f \quad (32)$$

$$(F_H)_{U_{\min}} = \frac{U_{\min}}{V} = \left\{ \frac{\tau_s \cos \alpha_e \cdot A}{\cos(\phi_e - \alpha_e)} + \frac{\tau_s \sin \beta \cos \alpha_e Q}{[\cos(\phi_e - \alpha_e + \beta) \cos(\phi_e - \alpha_e)]} \right\} \quad (33)$$

$$(R_t)_H = N_t \cos \alpha_{r2} \cdot \cos \alpha_a + (F_t)_{U_{\min}} \cdot \sin \alpha_e = (F_H)_{U_{\min}} \quad (34)$$

where the frictional force is determined by

$$F_t = \frac{\tau_s \sin \beta \cos \alpha_e Q}{[\cos(\phi_e + \beta - \alpha_e) \sin \phi_e]} \quad (35)$$

Therefore, N_t is rewritten as

$$N_t = \frac{[(F_H) - (F_t)_{U_{\min}} \sin \alpha_e]}{\cos \alpha_{r2} \cos \alpha_a} \quad (36)$$

The values of F_T and F_V are determined from the components of N_t and F_t . That is

$$F_T = -N_t \cos \alpha_{r2} \sin \alpha_a + F_t (\sin \eta_c \cos \alpha_a - \cos \eta_c \sin \alpha_{r2} \sin \alpha_a) \quad (37)$$

By contrast with the turning operation, as shown in Fig. 7, the workpiece carries out a rotary motion and the tool has a plane motion. The tooth path of a face-milling cutter is a cycloid as shown in Fig. 5. The comparison of tool geometry between the face milling cutter and turning tool is shown in Fig. 6. Where the radial angle, α_{r1} , the axial angle, α_a , and lead angle of face milling cutter are equal to the second normal side rake angle, α_{r2} , the back rake angle α_a and the side cutting edge angle, C_s , respectively.

$$t_1 = f_\theta \cos C_s \quad (38)$$

$$f_{\theta} = f \sin \theta_x \tag{39}$$

and

$$W = d / \cos C_s \tag{40}$$

where f = feedrate/(rev · per · tooth).

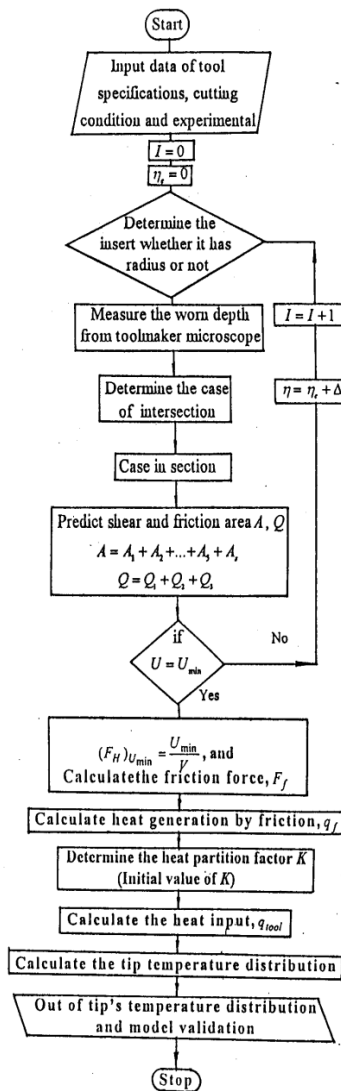


Figure 4: Flow chart of the inverse heat transfer solution

Figure 6 shows the unit chip cross section and various cutting force components exerted on workpiece at cutting edge where F_{HH} , F_{VV} and F_{TT} are equal to the cutting force components in turning. Thus the cutting forces are given by

$$F_X = F_{HH} \cos \theta_X + F_{VV} \sin \theta_X \tag{41}$$

$$F_Y = F_{HH} \sin \theta_X - F_{VV} \cos \theta_X \tag{42}$$

$$F_Z = F_{TT} \tag{43}$$

$$F_{VV} = (F_V)_M \cdot \cos C_s - (F_T)_M \cdot \sin C_s \tag{44}$$

$$F_{TT} = (F_T)_M \cdot \cos C_s + (F_V)_M \cdot \sin C_s \tag{45}$$

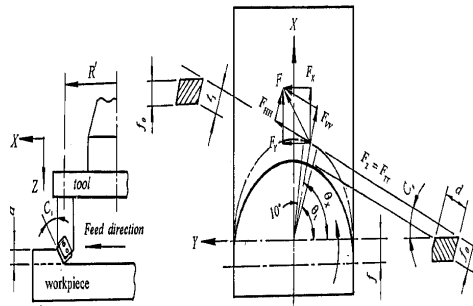


Figure 5: Cutting forces model of face milling

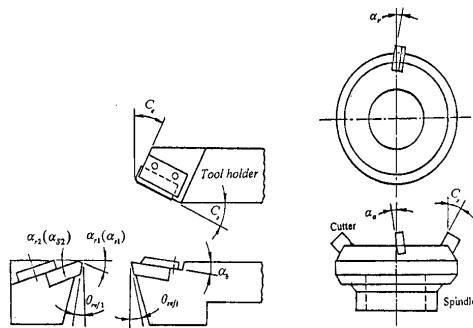


Figure 6: Tool geometric between (a) turning (b) milling cutter

2.2 Solid modeling of carbide tip

To develop a 3D finite element model for thermal analysis, a solid model of the tip can be established in three steps. First, the tip cross-section profile (TCSP) perpendicular to the main cutting edge was measured using a microscope, then CAD software, SolidWorks™, was used to generate the tip body by sweeping the TCSP along the main cutting edge with the specified pitch. Finally the tip's main cutting edge was simulated to remove unwanted material and create a solid model of turning tip geometry, as shown in Fig. 6.

2.3 Finite element model

The finite element mesh of the carbide tip is shown in Fig. 7, which was modeled by 58,000 four-node hexahedral elements. As shown in the top view of Fig. 8, 8×6 nodes are located on the projected contact length between the tool and the workpiece, 3×6 nodes are located on the chamfered width of the main cutting edge, and 1×6 nodes are placed on flank wear.

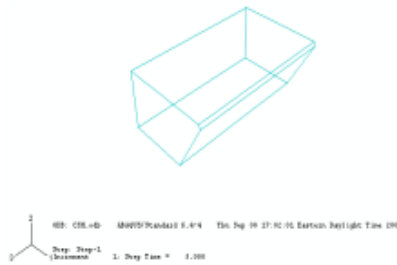


Figure 7: model chamfered edge tool

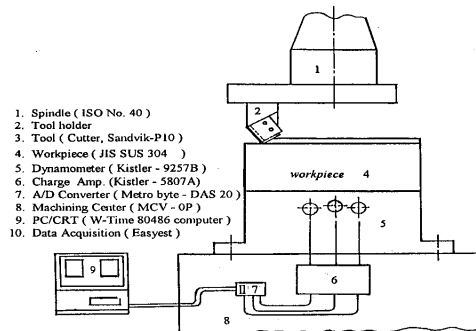


Figure 8: experimental cutting set-up

2.4 Modified carbide tip temperature model

Magnitude of the tip's load is shown in the following Eqs. (46) and (47)

$$K = \frac{U_f}{A'} \quad (46)$$

$$A' = L_p(d + W_e + V_b) \quad (47)$$

Where A' is the area of friction force action, U_f is the friction energy, W_e is the tip's chamfered width, d is the cutting depth, V_b is the flank wear of the tip and for simplification, the value of V_b is set to be 0.1mm. L_f is the contact length between the cutting edge and the workpiece (Eqs. 19), L_p is the projected contact length between the tool and the workpiece, as referred to in Fig. 3, and can be determined by Eq. 20 and the following conditions.

$$\rho c \frac{\partial T}{\partial t} = k \frac{\partial^2 T}{\partial x^2} + k \frac{\partial^2 T}{\partial y^2} + k \frac{\partial^2 T}{\partial z^2} \quad (48)$$

where ρ is the density, c is the thermal conductivity, and k is the heat capacity.

$$q_f = F_f V_c, q_{\text{tool}} = K q_f \quad [\text{Li and Shih (2005)}] \quad (49)$$

3 Experiment method and procedure

To verify these force models, experiments were conducted using the set-up in Fig. 8. In measuring the cutting forces a Kistler type 9257B, three-component piezoelectric dynamometer was used with a data acquisition system that consisted of Kistler type 5807A charge amplifiers, all measured data were recorded by a data acquisition system and analyzed by the control software (*Easyest*). The composition of workpiece is $C = 0.05\%$, $Mn = 1.17\%$, $P = 0.34\%$, $S = 0.24\%$, $Si = 0.29\%$, $Ni = 9.14\%$, $Cr = 18.45\%$, 168HB. The cutting tools used in the experiments are Sandvik p10, type *SIP* [Brookes (1992)]. Carbide-tipped tools: Back rake angle = 0° ; side rake angle = 6° ; end relief angle = 7° ; side relief angle = 9° ; end cutting edge angle = 70° ; side cutting angles = $20^\circ, 30^\circ, 40^\circ$; and nose radius = $0.0 \sim 0.1\text{mm}$.

4 Results and Discussion

4.1 The cutting forces

Fuh and Chang showed that increasing the side rake angles α_{r1} and α_{r2} , decreases the cutting forces F_{HH} , F_{VV} and F_{TT} as Ref. [Chang (2005)].

4.2 The cutting temperatures

Based on Li and Shih (2005), according to Eqs. (48) and (49), the flowchart for inverse heat transfer solution of K is described in Fig. 5.

The results obtained from the finite element analyses are shown in Figs. 9-10 and described as follows:

1. Fig. 9 shows the cutting temperatures vs. cutting time for different values C_s at $\alpha_{r1} = -30^\circ$ and $\alpha_{r2} = 30^\circ$ with a chamfered and an unchamfered sharp worn tool at $d = 2.00\text{mm}$, $f = .33\text{mm/rev}$, $V = 120\text{m/min}$ respectively.
2. Fig. 9 shows that the cutting edge temperature of the chamfered main edge sharp worn tool was lower than unchamfered main cutting edge worn tool.
3. Fig. 9 shows that the cutting temperatures of the chamfered main cutting edge worn tool is the lowest, when $C_s = 30^\circ$, $\alpha_{r1} = -30^\circ$ and $\alpha_{r2} = 30^\circ$, and the temperature does not exceed 410°C .
4. Fig. 10, shows that the distribution of chamfered main cutting edge worn tool's temperature was close to Fig. 8

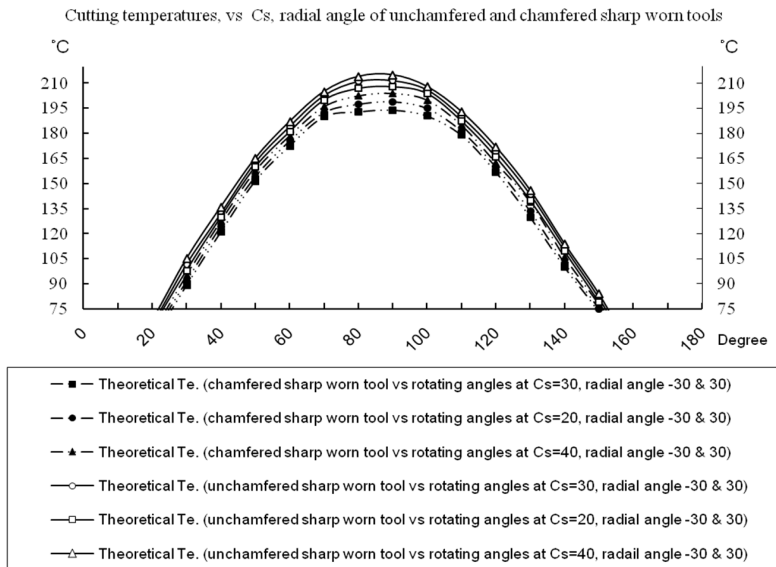


Figure 9: shows the cutting temperatures vs. cutting time for different values α_{r1} and α_{r2} with a chamfered and an unchamfered sharp worn tool at $d = 2.0\text{mm}$, $f = .33\text{mm/rev}$, $V = 120\text{m/min}$ at 30° respectively.

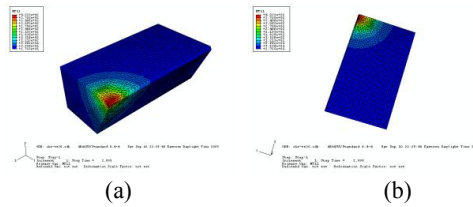


Figure 10: Temperature distribution with chamfered cutting edge worn inserts (a) heat flux (b) near the tool nose at $C_s = 30^\circ$ and $\alpha_{r1} = -30^\circ$, $\alpha_{r2} = 30^\circ$, $d = 2.0\text{mm}$, $f = 0.33\text{mm/rev}$, and $V = 120\text{m/min}$ (stainless steel)

5 Conclusions

Good correlations were obtained between predicted values and experimental results of forces during milling stainless steel with sharp tools [Chang (2005)]. A new model for sharp worn tools with chamfered main cutting edge has been developed by including the variation of shear plane areas. In this model, the energy method is also used to more accurately predict cutting force. The FEM and Inverse heat transfer solution for tool temperature in stainless milling is obtained and compared with experimental measurements. The good agreement demonstrates the accuracy of proposed model.

Acknowledgement: The National Science Council, Taiwan, R.O.C. supported the work under grant No. NSC-100-2221-E-197-011

References

- Brookes, K. J. A.** (1992): *World Directory and Handbook of Hard metals*. International carbide data hand book, United Kingdom, 5th edition.
- Chang, C. S.** (2005): Prediction of cutting forces in milling stainless steels using chamfered main cutting edge tool. *Journal of Mechanics (SCI)*, pp. 145–155.
- Chang, C. S.** (2007): Prediction of the cutting temperatures of stainless steel with chamfered main cutting edge tools. *J. of Materials Processing Technology*, vol. 190, no. 1-3, pp. 332–341.
- Leshock, C. E.; Shin, Y. C.** (1997): Investigation on cutting temperature in turning by a toolwork thermocouple technique. *ASME J. Manuf. Sci. Eng.*, vol. 119, pp. 502.
- Li, R.; Shih, A. J.** (2005): *Inverse heat transfer solution in tool temperature titanium drilling, mechanical engineering*. University of Michigan, Ann Arbor.

Singamneni, S. B. (2005): A mixed solution for three-dimensional temperature distribution in turning inserts using finite and boundary element techniques. *J. of Materials Processing Technology*, vol. 166, pp. 98–106.

Tay, A. O.; Stevenson, M. G.; de Vahl Davis, G.; Oxley, P. L. B. (1976): A numerical method for calculating temperature distributions in machining from force and shear angle measurements. *Int. J. Machine Tool Des. Res.*, vol. 16, pp. 335.

